# Transient Electron Thermal Transport Analysis Accounting Oblique Electron Cyclotron Resonance Heating Injection to Magnetic Field Line

Tatsuya KOBAYASHI[1,2)], Ryoma YANAI[1)], Toru Ii TSUJIMURA[1)], Tokihiko TOKUZAWA[1,2)], Yasuo YOSHIMURA[1)], Katsumi IDA[1)] and the LHD Experiment Group

[1)]*National Institute for Fusion Science, National Institutes of Natural Sciences, Toki 509-5292, Japan*
[2)]*The Graduate University for Advanced Studies, SOKENDAI, Toki 509-5292, Japan*

(Received 12 July 2020 / Accepted 27 August 2020)

In response to recent upgrade of the raytracing code for the electron cyclotron resonance heating (ECH) in LHD, transient electron thermal transport is reanalyzed. The upgraded code *LHDGauss-U* takes into account the oblique injection of the ECH ray to magnetic field line. The obtained results show reduced transport hysteresis widths by up to $\sim$ 20% where the heating absorption is less significant, but qualitative features of the transport hysteresis reported in previous studies are found to be preserved.



Keywords: thermal transport, turbulence, modulation ECH, transport hysteresis, isotope effect

DOI: 10.1585/pfr.15.1402072

## 1. Introduction

One of the ultimate goals of plasma physics research is to obtain a reasonable model for plasma thermal transport. It is believed that the heat flux in magnetically confined high temperature plasmas cannot be expressed by the simplest "Fick's law", where the heat flux is modeled to be proportional to the local temperature gradient [1]. Instead, a wide variety of models, including the diffusion-convection model [2–5], the critical gradient model [6, 7], nonlocal models [8–14], models including off-diagonal contribution [15–17], and others were developed for comprehensively describing the complicated transport phenomena.

Electron transient heat flux components having two different time scales were found in modulation electron cyclotron resonance heating (ECH) experiments. They are the conventional diffusion flux that slowly varies with the local gradient and a nonlocal flux that quickly increases (decreases) when the ECH is turned-on (turned-off). The latter component evolves independently of the local gradient but with the injected ECH power. Therefore, trajectories in the flux-gradient relation when the ECH is applied or not applied tend to differ, drawing a hysteresis loop when the nonlocal heat flux component is prominent [12–14, 18, 19].

Analysis of the heat flux evolution is performed based on the measured electron temperature response to the modulation ECH and the calculated ECH absorption profile by raytracing codes. Recently the raytracing code for LHD, *LHDGauss* [20], is upgraded. The new raytracing code *LHDGauss-U* accounts for the oblique injection of rays to magnetic field line in the ECH absorption coefficient calculation [21]. In this paper, heat flux evolution shown in [14] is reanalyzed using *LHDGauss-U*. Although the hysteresis trajectory previously obtained slightly shrinks by up to $\sim$ 20% where the heating absorption is less significant, qualitative features of the transport hysteresis presented in [14] are preserved.

## 2. Results

Figure 1 shows the ECH injection configuration on (a) poloidal cross section and (b) top view. The ECH focal point is expressed on a target plane, the plane perpendicular to the major radius at $R = 3.9$ m in front of the ECH injection port (the outer port # 2). The horizontal and vertical coordinates of the focal point are denoted as $T_f$ and $Z_f$, respectively. With a toroidal magnetic field strength of $B_t = 2.75$ T (the standard field strength), the 77 GHz microwave for the ECH does not have the resonance in front of the launcher as shown in Fig. 1 (b). To meet the resonance with the ordinary-mode heating, the launcher must be directed toward either toroidal directions. With this oblique injection operation, the heating beam has a finite angle with respect to magnetic field line. For taking into account the oblique injection of ECH to magnetic field line in the absorption coefficient calculation [21], an upgrade is performed for *LHDGauss* code. Now the new code in which the oblique injection of ECH is accounted is called *LHDGauss-U* hereafter. Validity of *LHDGauss-U* is examined by the modulation ECH experiment, where a more reliable ECH absorption profile being similar to the

*author's e-mail: kobayashi.tatsuya@nifs.ac.jp*

modulation phase delay profile is obtained by *LHDGauss-U*.

Transport analysis is performed for the dataset of the isotope effect study [14]. Three representative shots having different D/H ratio of 89% (# 146822), 60% (# 147882), and 4% (# 152229) are focused upon. They are called the D plasma, the mixed plasma, and the H plasma, respectively. Here, the D/H ratio is evaluated as $I_{D_\alpha}/(I_{D_\alpha} + I_{H_\alpha})$, where $I_{D_\alpha}$ and $I_{H_\alpha}$ are the intensities of the $D_\alpha$ emission and the $H_\alpha$ emission measured by a passive spectroscopy, respectively. The experimental conditions are as follows: the magnetic field strength of $B_t = 2.75$ T, the magnetic axis of $R_{ax} = 3.6$ m, the NBI power of $P_{NB} = 3.6$ MW (balanced) for the base plasma sustainment, and the line averaged density of $\bar{n}_e \sim 1.3 \times 10^{19}$ m$^{-3}$. Modulation ECH of $\sim$ 1 MW rectangular waveform with the frequency of 23 Hz is applied by a 77 GHz gyrotron. Electron temperature response synchronizing the modulation ECH is diagnosed by an electron cyclotron emission (ECE) radiometer system.

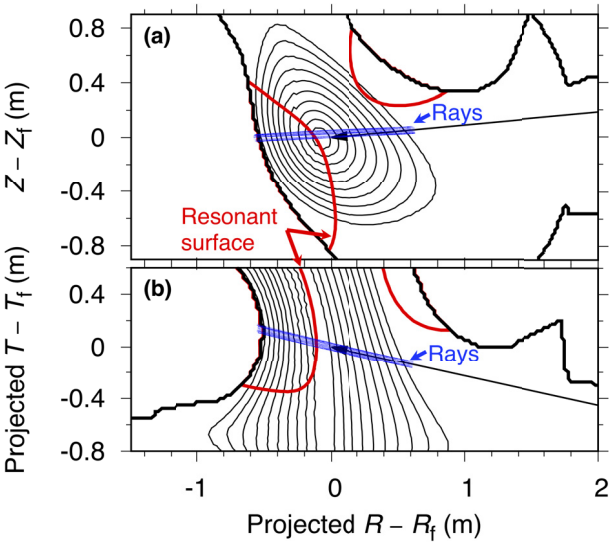


Fig. 1 Schematics of ECH injection configuration on (a) poloidal cross section and (b) top view. Magnetic surfaces and resonant surfaces correspond to slices along the ECH rays.

Long-time averaged profiles of the electron temperature and the electron density are shown in the first row of Fig. 2. Density profile is almost identical for three shots, and characterized by a hollow shape. Peaking of the electron temperature is more visible as the deuterium content increases, likely due to easily formed electron internal transport barrier in deuterium plasmas by an isotope effect [14]. The ECH absorption profiles are calculated by two ray tracing codes, *LHDGauss* (conventional) and *LHDGauss-U* (oblique injection accounted) as shown in the second row of Fig. 2. Compared to the results of *LHDGauss*, the ECH absorption power density profile calculated with *LHDGauss-U* shows a prominent peak in the core region ($r_{eff} < 0.05$ m) and a long tail in the outer radii ($r_{eff} > 0.15$ m). However, due to a small contribution of core quantities to the volume integral, the power absorption profile is extended up to approximately $r_{eff} \sim 0.3$ m. In

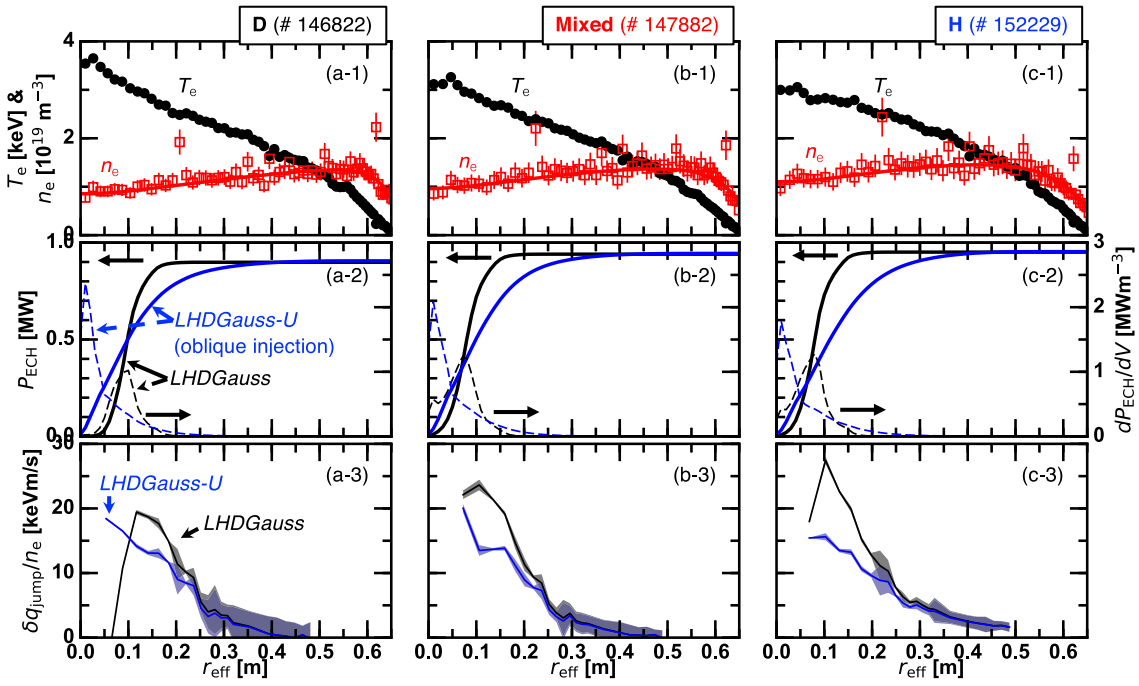


Fig. 2 Radial profiles of electron temperature and electron density (first row), ECH absorption power and power density calculated by raytracing codes (second row), and the transport hysteresis width (third row) for (a) D, (b) Mixed, and (c) H plasmas.

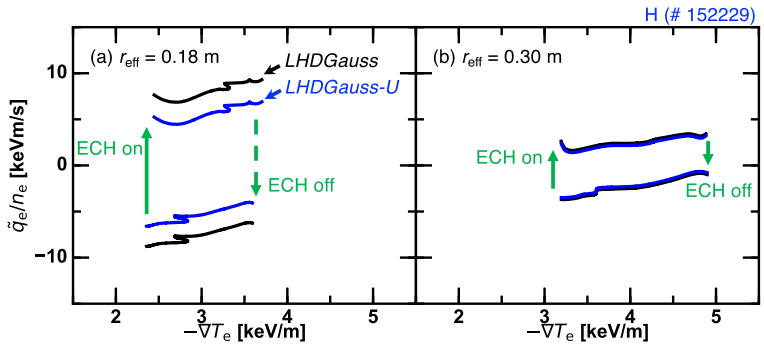


Fig. 3 Flux-gradient diagram at (a) $r_{\rm eff}$ = 0.18 m and (b) $r_{\rm eff}$ = 0.30 m calculated with *LHDGauss* and *LHDGauss-U*.

*LHDGauss-U*, the realistic angle between the ECH ray and the local magnetic field line is used in the ECH absorption coefficient calculation, which makes the deposition profile more reliable. Total absorption power remains unchanged before and after the code upgrade. Since the ECH absorption profile is directly used in calculating the heat flux profile as shown by Eq. (1) in [14], the transport characteristics are reanalyzed with the newly developed raytracing code.

Flux-gradient relation diagram for the hydrogen plasma # 152229 is shown in Fig. 3 as an example. Here, the vertical axes correspond to the fluctuation part of the electron heat flux divided by the mean local electron density, $\tilde{q}_e/n_e$. Cases of two radial positions are shown, $r_{\rm eff}$ = 0.18 m and $r_{\rm eff}$ = 0.30 m. They correspond to the locations where the extended tail of the ECH absorption profile calculated by *LHDGauss-U* emerges and the ECH deposition is absent in both codes, respectively. The former case shown in Fig. 3 (a) exhibits a distinguishable difference between the results obtained by *LHDGauss* and *LHDGauss-U*. The hysteresis loop taking into account the effect of the oblique ECH injection shrinks by $\sim$ 25%. However, a finite hysteresis width still remains, suggesting the direct impact of the heating application to the transport not through the local gradient. The hysteresis widths are almost identical where the ECH absorption is absent in both codes as shown in Fig. 3 (b).

The third row of Fig. 2 shows the radial profile of the transport hysteresis width divided by the mean electron density, $\delta q_{\rm jump}/n_e$. The difference between two results is substantial where the ECH absorption profiles calculated by *LHDGauss* and *LHDGauss-U* are different. The difference becomes almost invisible in the outer radial locations, i.e., $r_{\rm eff} > 0.25$ m. By using the *LHDGauss-U* absorption profile, the transport hysteresis width profiles become monotonic decay functions of the radius.

Figure 4 shows the ratio of the transport hysteresis width calculated by *LHDGauss-U* to that calculated by *LHDGauss*. The hysteresis width is reduced by $\sim$ 20% at $r_{\rm eff}$ = 0.2 m, and approaches to unity as the radius increases. It turns out that the hysteresis width has been systematically overestimated by the perpendicular ECH absorption assumption of *LHDGauss*, which is now corrected

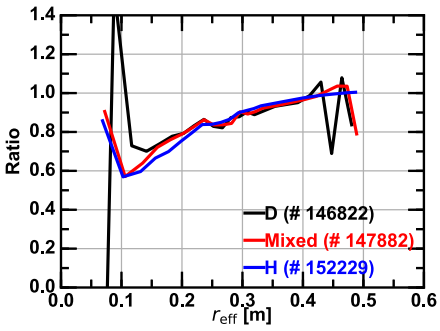


Fig. 4 Radial profile of ratio of the transport hysteresis width calculated by *LHDGauss-U* to that calculated by *LHDGauss*.

by using *LHDGauss-U*. The ratio is approximately independent on the plasma deuterium content. Therefore, qualitative features of the transport hysteresis presented in [14], i.e., hysteresis width independent on the hydrogen isotope fuel contents, is preserved.

## 3. Summary

In this paper, the heat flux induced by the modulation ECH was reanalyzed based on a new raytracing code *LHDGauss-U*, which accounted for the oblique injection of the ECH ray to magnetic field line. A wider ECH absorption profile was obtained by *LHDGauss-U* compared to a conventional code *LHDGauss*, which potentially influences the heat flux analysis. By drawing the flux-gradient relation obtained with *LHDGauss-U*, hysteresis widths reduced by up to $\sim$ 20% where the heating absorption was less significant. The reduction rate of the hysteresis width was less sensitive to the plasma deuterium content. Qualitative features of the transport hysteresis reported in previous studies were therefore found to be maintained even if the oblique injection of the ECH ray to magnetic field line was taken into account.

## Acknowledgments

We thank S. Kubo, K. Tanaka, K. Itoh, and S.

Sakakibara for strong support. This work is partly supported by the National Institute for Fusion Science grants (ULHH033) and by the Grant-in-Aid for Scientific Research of JSPS (17K14898).

[1] N.J. Lopes Cardozo, Plasma Phys. Control. Fusion **37**, 799 (1995).
[2] T.C. Luce, C.C. Petty and J.C.M. De Haas, Phys. Rev. Lett. **68**, 52 (1992).
[3] P. Mantica, G. Gorini, G.M.D. Hogeweij, N.J. Lopes Cardozo and A.M.R. Schilham, Phys. Rev. Lett. **85**, 4534 (2000).
[4] P. Mantica, F. Ryter, C. Capuano, H.U. Fahrbach, F. Leuterer, W. Suttrop, J. Weiland and ASDEX-Upgrade Team, Plasma Phys. Control. Fusion **48**, 385 (2006).
[5] S.D. Song, X.L. Zou, G. Giruzzi, W.W. Xiao, X.T. Ding, B.J. Ding, J.L. Ségui, D. Elbèze, F. Clairet, C. Fenzi *et al.*, Nucl. Fusion **52**, 033006 (2012).
[6] F. Ryter, G. Tardini, F. De Luca, H.-U. Fahrbach, F. Imbeaux, A. Jacchia, K.K. Kirov, F. Leuterer, P. Mantica, A.G. Peeters *et al.*, Nucl. Fusion **43**, 1396 (2003).
[7] J.C. DeBoo, C.C. Petty, A.E. White, K.H. Burrell, E.J. Doyle, J.C. Hillesheim, C. Holland, G.R. McKee, T.L. Rhodes, L. Schmitz *et al.*, Phys. Plasmas **19**, 082518 (2012).
[8] E.D. Fredrickson, K. McGuire, A. Cavallo, R. Budny, A. Janos, D. Monticello, Y. Nagayama, W. Park, G. Taylor and M.C. Zarnstorff, Phys. Rev. Lett. **65**, 2869 (1990).
[9] M.W. Kissick, E.D. Fredrickson, J.D. Callen, C.E. Bush, Z. Chang, P.C. Efthimion, R.A. Hulse, D.K. Mansfield, H.K. Park, J.F. Schivell *et al.*, Nucl. Fusion **34**, 349 (1994).
[10] K.W. Gentle, W.L. Rowan, R.V. Bravenec, G. Cima, T.P. Crowley, H. Gasquet, G.A. Hallock, J. Heard, A. Ouroua, P.E. Phillips, D.W. Ross, P.M. Schoch and C. Watts, Phys. Rev. Lett. **74**, 3620 (1995).
[11] U. Stroth, L. Giannone, H.J. Hartfuss, E.C.H. Group *et al.*, Plasma Phys. Control. Fusion **38**, 611 (1996).
[12] S. Inagaki, T. Tokuzawa, N. Tamura, S.-I. Itoh, T. Kobayashi, K. Ida, T. Shimozuma, S. Kubo, K. Tanaka, T. Ido *et al.*, Nucl. Fusion **53**, 113006 (2013).
[13] T. Kobayashi, K. Ida, T. Ii Tsujimura, S. Inagaki, T. Tokuzawa, H. Tsuchiya, N. Tamura, H. Igami, Y. Yoshimura, S.-I. Itoh *et al.*, Nucl. Fusion **58**, 126031 (2018).
[14] T. Kobayashi, K. Ida, K. Tanaka, M. Yoshinuma, T. Ii Tsujimura, S. Inagaki, T. Tokuzawa, H. Tsuchiya, N. Tamura, H. Igami *et al.*, Nucl. Fusion **60**, 076015 (2020).
[15] P. Rodriguez-Fernandez, A.E. White, N.T. Howard, B.A. Grierson, G.M. Staebler, J.E. Rice, X. Yuan, N.M. Cao, A.J. Creely, M.J. Greenwald *et al.*, Phys. Rev. Lett. **120**, 075001 (2018).
[16] P. Rodriguez-Fernandez, A.E. White, N.T. Howard, B.A. Grierson, L. Zeng, X. Yuan, G.M. Staebler, M.E. Austin, T. Odstrcil, T.L. Rhodes *et al.*, Phys. Plasmas **26**, 062503 (2019).
[17] C. Angioni, E. Fable, F. Ryter, P. Rodriguez-Fernandez, T. Pütterich *et al.*, Nucl. Fusion **59**, 106007 (2019).
[18] S.-I. Itoh and K. Itoh, Sci. Rep. **2**, 860 (2012).
[19] S.-I. Itoh, K. Itoh and S. Inagaki, Nucl. Fusion **57**, 022003 (2016).
[20] T. Ii Tsujimura, S. Kubo, H. Takahashi, R. Makino, R. Seki, Y. Yoshimura, H. Igami, T. Shimozuma, K. Ida, C. Suzuki *et al.*, Nucl. Fusion **55**, 123019 (2015).
[21] F. Volpe, Phys. Plasmas **14**, 122105 (2007).